Electronic circular dichroism in exciton-coupled dimers: Vibronic spectra from a general all-coordinates quantum-dynamical approach

SUPPORTING INFORMATION

DANIELE PADULA,[a] DAVID PICCONI,[b,c] ALESSANDRO LAMI,[d] GENNARO PESCITELLI,[a] FABRIZIO SANTORO[d]

[a]*Dipartimento di Chimica e Chimica Industriale, Università degli Studi di Pisa, via Risorgimento 35, I-56126 Pisa, Italy*

[b]*Scuola Normale Superiore di Pisa, Piazza dei Cavalieri 7, I-56126 Pisa, Italy*

[c]*Department of Chemistry, Technische Universität München, Lichtenbergstr. 4, D-85747 Garching, Germany*

[d]*Consiglio Nazionale delle Ricerche – CNR, Istituto di Chimica dei Composti Organo Metallici (ICCOM-CNR), UOS di Pisa, Area della Ricerca, Via G. Moruzzi 1, I-56124 Pisa, Italy*

* Correspondence to: fabrizio.santoro@iccom.cnr.it

1. Theory

1.1 Derivatives of the adiabatic energies from the vibronic model

Starting from Eq. 7 in the manuscript it is straightforward to obtain the first derivatives with respect to symmetric and anti-symmetric coordinates

$$\frac{\partial E_{Ad\pm}(\boldsymbol{Q_d})}{\partial Q_{j+}} = \frac{1}{2}\sum_{\boldsymbol{k}}\left(\boldsymbol{b}+\boldsymbol{\omega^2}\right)_{j+,k+} Q_{k+} + \lambda_j \,/\sqrt{2} \mp \frac{\left(\frac{1}{2}\boldsymbol{Q}_-^T(\boldsymbol{b}-\boldsymbol{\omega^2})\boldsymbol{Q}_+ - \boldsymbol{\lambda}^T\boldsymbol{Q}_-/\sqrt{2}\right)\left(\frac{1}{2}\sum_{\boldsymbol{k}}(\boldsymbol{b}-\boldsymbol{\omega^2})_{k-,j+}Q_{k+}\right)}{\sqrt{\left[\frac{1}{2}\boldsymbol{Q}_-^T(\boldsymbol{b}-\boldsymbol{\omega^2})\boldsymbol{Q}_+ - \boldsymbol{\lambda}^T\boldsymbol{Q}_-/\sqrt{2}\right]^2 + V_{12}^2}} \qquad (1a)$$

$$\frac{\partial E_{Ad\pm}(\boldsymbol{Q_d})}{\partial Q_{j-}} = \frac{1}{2}\sum_{\boldsymbol{k}}(\boldsymbol{b}+\boldsymbol{\omega^2})_{j-,k-} Q_{k-} \mp \frac{\left(\frac{1}{2}\boldsymbol{Q}_-^T(\boldsymbol{b}-\boldsymbol{\omega^2})\boldsymbol{Q}_+ - \boldsymbol{\lambda}^T\boldsymbol{Q}_-/\sqrt{2}\right)\left(\frac{1}{2}\sum_{\boldsymbol{k}}(\boldsymbol{b}-\boldsymbol{\omega^2})_{j-,k+}Q_{k+} - \lambda_j\,/\sqrt{2}\right)}{\sqrt{\left[\frac{1}{2}\boldsymbol{Q}_-^T(\boldsymbol{b}-\boldsymbol{\omega^2})\boldsymbol{Q}_+ - \boldsymbol{\lambda}^T\boldsymbol{Q}_-/\sqrt{2}\right]^2 + V_{12}^2}} \qquad (1b)$$

The calculation of second derivatives is straightforward too but their expression is rather long. For what is needed in the manuscript it is enough to give only the second derivative with respect to anti-symmetric coordinates in C_2 symmetry $\boldsymbol{Q}_- = \boldsymbol{0}$

$$\left(\frac{\partial^2 E_{Ad\pm}(\boldsymbol{Q_d})}{\partial Q_{j-}Q_{l-}}\right)_{\boldsymbol{Q}_-=\boldsymbol{0}} = \frac{1}{2}(\boldsymbol{b}+\boldsymbol{\omega^2})_{j-,l-} + \mp\frac{V_{12}\left(\frac{1}{2}\sum_{\boldsymbol{k}}(\boldsymbol{b}-\boldsymbol{\omega^2})_{j-,k+}Q_{k+} - \lambda_j\,/\sqrt{2}\right)\left(\frac{1}{2}\sum_{\boldsymbol{k'}}(\boldsymbol{b}-\boldsymbol{\omega^2})_{l-,k'+}Q_{k'+} - \lambda_l\,/\sqrt{2}\right)}{V_{12}^2}$$

$$\pm\frac{\left(\frac{1}{2}\boldsymbol{Q}_-^T(\boldsymbol{b}-\boldsymbol{\omega^2})\boldsymbol{Q}_+ - \boldsymbol{\lambda}^T\boldsymbol{Q}_-/\sqrt{2}\right)^2\left(\frac{1}{2}\sum_{\boldsymbol{k}}(\boldsymbol{b}-\boldsymbol{\omega^2})_{j-,k+}Q_{k+} - \lambda_j\,/\sqrt{2}\right)\left(\frac{1}{2}\sum_{\boldsymbol{k'}}(\boldsymbol{b}-\boldsymbol{\omega^2})_{l-,k'+}Q_{k'+} - \lambda_l\,/\sqrt{2}\right)}{V_{12}^2} \qquad (2)$$

1.2 Hierarchical representation

The *n*-the group of modes of the QVC hierarchy is generally defined as

$$\begin{cases} j = 1, 2^n \\ \mathbf{q}_j^{(n)} = N\left[\boldsymbol{F_1}\mathbf{q}_j^{(n-1)} - \boldsymbol{P_{n-1}P_{n-2}F_1}\mathbf{q}_j^{(n-1)} - \sum_{k<j}\mathbf{q}_k^{(n)}\left(\mathbf{q}_k^{(n)}\right)^T \boldsymbol{F_1}\mathbf{q}_j^{(n-1)}\right] \\ \mathbf{q}_{j+2^n}^{(n)} = N\left[\boldsymbol{F_2}\mathbf{q}_j^{(n-1)} - \boldsymbol{P_{n-1}P_{n-2}F_2}\mathbf{q}_j^{(n-1)} - \sum_{k<j+2^n}\mathbf{q}_k^{(n)}\left(\mathbf{q}_k^{(n)}\right)^T \boldsymbol{F_2}\mathbf{q}_j^{(n-1)}\right] \end{cases} \quad (3)$$

Consider now the limiting case of the LVC Hamiltonian $\boldsymbol{b} = \boldsymbol{\omega^2}$,and the expression of the L_1 and L_2 PES V_{L1} and V_{L2} in the new coordinates obtained from the orthogonal transformation of the dimensionless ground-state coordinates that generate the hierarchical representation

$$\mathcal{H}_{L1} = E_o + \overline{\boldsymbol{\Lambda}}_1^T\boldsymbol{q_d} + \frac{1}{2}\boldsymbol{q}_d^T\overline{\boldsymbol{\Omega}}\boldsymbol{q_d} \quad (4a)$$

$$\mathcal{H}_{L2} = E_o + \overline{\boldsymbol{\Lambda}}_2^T\boldsymbol{q_d} + \frac{1}{2}\boldsymbol{q}_d^T\overline{\boldsymbol{\Omega}}\boldsymbol{q_d} \quad (4b)$$

where $\overline{\boldsymbol{\Lambda}}_1^T = \left(\overline{\boldsymbol{\lambda}}^{\boldsymbol{T}}, \mathbf{0}^{\boldsymbol{T}}\right)$, $\overline{\boldsymbol{\Lambda}}_2^T = \left(\mathbf{0}^{\boldsymbol{T}}, \overline{\boldsymbol{\lambda}}^{\boldsymbol{T}}\right)$ and by construction $\overline{\boldsymbol{\lambda}}^{\boldsymbol{T}} = (\lambda_1, 0,0, \ldots 0)$

$$\left(\frac{\partial^2 E_{Ad\pm}(\boldsymbol{Q_d})}{\partial Q_{j-}Q_{l-}}\right)_{\boldsymbol{Q_-=0}} = (\overline{\boldsymbol{\Omega}})_{j-,l-} \mp \frac{\overline{\lambda}_1^2}{2V_{\mathbf{12}}}\delta_{1,j}\delta_{j,l} \quad (5)$$

The diagonal force constant along mode is therefore negative if

$$V_{12} < \frac{\overline{\lambda}_1^2}{2\overline{\Omega}_{1,1}} \quad (6)$$

where $\overline{\lambda}_1^2/\left(2\overline{\Omega}_{1,1}\right) = E_{r1} \equiv E_{r2}$ is the reorganization energy on the harmonic PES of the excited state of the monomer along the first (second) coordinate of the hierarchy q_1 (q_2), i.e. the two coordinates that concentrate all the linear terms in the Hamiltonians $\mathcal{H}_{L1}$ and $\mathcal{H}_{L2}$, respectively. Eq.6 is a sufficient (but not necessary) condition to have an imaginary frequency on the lower

energy adiabatic PES along a non-total symmetric coordinate. Notice that $\bar{\lambda}_1^2/(2\bar{\Omega}_{1,1})$ is clearly a lower bound of the total reorganization energy of the monomer.

1.3 Analytical expression of the first cumulants of the spectra

Here we illustrate the reason why the reduced-dimensionality models described in Section 2.3 in the main text are expected to be suitable for the computation of the spectra.

In particular, we refer to the one-photon absorption spectrum, but analogous considerations hold also for ECD. In Section 2.2 it was proved that the spectrum can be computed through a quantum dynamical simulation, by Fourier transforming the quantity

$$P(t) = \left\langle L_1; \mathbf{0} \middle| e^{-i\frac{\mathcal{H}t}{\hbar}} \middle| L_1; \mathbf{0} \right\rangle + cos\beta \left\langle L_1; \mathbf{0} \middle| e^{-i\frac{\mathcal{H}t}{\hbar}} \middle| L_2; \mathbf{0} \right\rangle \quad (4)$$

Focusing on the short time behavior of the system we expand the logarithm of $P(t)$ around $= 0$:

$$ln\, P(t) \;=\; \sum_{k=0}^{\infty} \frac{(-it)^k}{\hbar^k k!} C_k \quad (5)$$

The coefficients C_k are denoted cumulants, and are directly related to the spectrum. In practice, C_1 , C_2 and C_3 represent the center of gravity, the width and the asymmetry of the spectrum, respectively. They can be computed evaluating the moments

$$M_n = \langle L_1; 0|\mathcal{H}^n|L_1; 0\rangle + cos\beta\langle L_1; 0|\mathcal{H}^n|L_2; 0\rangle \quad (6)$$

and using the relations:

$$C_1 = M_1 \quad (7a)$$

$$C_2 = M_2 \; - M_1^2 \quad (7b)$$

$$C_3 = M_3 - 3M_2M_1 + 2M_1^3 \quad (7c)$$

All these quantities can be computed analytically for the QVC Hamiltonian (Eq. 5), in a straightforward manner, as indicated in Ref. [54] in the main text.

Here we report only the final expressions so to illustrate which terms are missing in the reduced models. With the nomenclature of Sec. 2.3 we have, for the first cumulant,

$$C_1 = E_0 + \frac{1}{2}\mathrm{Tr}[\mathbf{c}+3\boldsymbol{\omega}] + V_{12}cos\beta \quad (8)$$

and this value is reproduced exactly already in the 2D reduced-dimensionality model arising from the first-block of the hierarchy, where the matrices **c** and **ω** are first transformed and then truncated first. In fact, it suffices adding appropriate constants to the diabatic surfaces to recover the trace of **c**+3**ω**.

The expressions for the second and the third cumulants are

$$C_2 = sin^2\beta\, V_{12} + \frac{1}{2}\boldsymbol{\lambda}^T\boldsymbol{\lambda} + \frac{1}{8}\mathrm{Tr}[(\mathbf{c}-\boldsymbol{\omega})^2] \quad (9)$$

$$\mathrm{C}_3 = \frac{1}{4}\boldsymbol{\lambda}^{\mathrm{T}}(3\mathbf{c}-\boldsymbol{\omega})\boldsymbol{\lambda} + 2cos^3\beta V_{12}^3 - \frac{cos\beta}{2}V_{12}\boldsymbol{\lambda}^T\boldsymbol{\lambda} \quad (10)$$
$$+\frac{1}{8}\mathrm{Tr}[(\mathbf{c}-\boldsymbol{\omega})(\mathbf{c}+\boldsymbol{\omega})(\mathbf{c}-\boldsymbol{\omega})] - \frac{cos\beta}{2}\mathrm{V}_{12}\mathrm{Tr}[(\mathbf{c}-\boldsymbol{\omega})^2]$$

In these quantities, all the terms involving the parameters E_0 , V_{12} and $\boldsymbol{\lambda}$ are recovered with any truncation of the hierarchy, because the transformed $\boldsymbol{\lambda}$ vector is concentrated on the first two effective modes, defining the first hierarchical block. On the contrary the terms involving only the matrices **c** and **ω** (those with the trace operation), once transformed and truncated, are recovered only partially, depending on the member of the hierarchy. However, as explicitly shown in Ref. [54], the errors are small, since they depend on the difference **c - ω**, and the elements of these two matrices are of the same order of magnitude.

2. Results

2.1 Testing the reliability of the vibronic model

Table S1 shows the monomer and dimer modes undergoing largest dimensionless shifts (δ) from ground to excited state geometries, and their correlation with the dimer modes mostly displaced from the ground-state to the minS_1-*loc* structure. It can be seen that in most of the cases it can be established a clear correlation between monomer and dimer modes, that show very similar frequencies and displacements. Notice in fact that, given a pair of modes, one on each monomer with a displacement δ, in the ideal case in which they generate a pair of dimer modes that are simply their symmetric and anti-symmetric combinations, they should exhibit displacements $\pm\delta/\sqrt{2}$ at the minima of the local diabatic excitations, and a displacement somewhat smaller at the S_1 global minimum minS_1-*loc*, where a residual mixing with the other excitation still exists. These facts support the reliability of the model even if some deviations are unavoidable and are evidenced for instance by the inability to establish the correlation for some modes, because of the mixing among almost degenerate vibrations in the dimer, and by the moderate differences of the absolute values of the displacements along the pair of *a*- and *b*-symmetry modes.

As we pointed out, our vibronic model provides an analytical expression of the S_1 and S_2 energy PESs of the dimer, giving us the possibility to test its reliability concerning both geometries and energies at relevant structures. Table S2 shows that, as predicted from the model, minS_1-C_2 and minS_2-C_2 show quite similar structures, and that the displacements between the FC minS_1-*loc* geometries are very similar to those from the ground and L_a minima in the monomer. Moreover, the energy difference from FC structure to minS_1-*loc* is predicted to be 1645 cm^{-1} to be compared with the value 1750 cm^{-1} obtained by CAM-B3LYP direct calculation.

The saddle point minS_1-C_2 is predicted to be 515 cm^{-1} above the global minimum minS_1-*loc* which also compares very nicely with the 525 cm^{-1} value obtained from electronic calculations. Further support to the reliability of the vibronic model comes from inspection of Table S3 showing that the electric transition dipoles predicted by the vibronic model in its S_0 geometry (minS_0-mod, corresponding to have both the monomers in their ground-state structure) and in the L_2 minimum (minL_2) are very similar to those directly computed for the dimer by TD-DFT at the ground-state minS_0 and minS_1-*loc* geometries.

2.2 Dependence of the spectra on the exciton coupling

In order to investigate the possible effect of an error in the estimation of the exciton coupling, and of the neglect of its dependence on nuclear coordinates, in Figure S6 we report the spectra computed according to the same data used in Figure 6 in the main text, apart from the coupling V_{12} that has been reduced by a factor 4 (-85 cm^{-1}, a value similar to what estimated by Harada *et al. ref* [26] in the main text), and increased by a factor 2 (-680 cm^{-1}). Intermediate values of V_{12} give results easily guessed by interpolation and are not reported for the sake of brevity. It can be noticed that increasing the coupling to -680 cm^{-1} produces a remarkable increase of the splitting of the vibronic bands (750 and 850 cm^{-1} in ECD and 1940 cm^{-1} in absorption) worsening the agreement with experiment; on the contrary, the reduction of the coupling to -85 cm^{-1} reduces the splitting slightly (715 and 735 cm^{-1} in ECD and 1530 cm^{-1} in absorption), only modestly improving the comparison with experiment.

Table S1. Monomer and dimer normal modes mainly shifted in the considered electronic transitions. For the dimer 1 the displacements from FC geometry to minS_1-*loc* are considered. Displacements δ are given in dimensionless coordinates

Anthracene			**Dimer**			
Normal mode	Frequency (S_0, cm^{-1})	δ ($2^{-1/2}\delta$)	Normal mode	Frequency (S_0, cm^{-1})	δ	Symmetry
38	1181	-0.46	89	1188	-0.18	B
		(-0.33)	not detectable because of mixing			A
41	1292	-0.47	100	1297	-0.16	B
		(-0.33)	101	1301	-0.19	A
43	1310	-0.63	102	1305	0.36	B
		(-0.45)	103	1328	-0.30	A
48	1488	1.18	116	1483	0.75	B
		(0.83)	117	1486	-0.77	A
53	1655	0.94	127	1650	-0.59	B
		(0.66)	128	1653	-0.67	A

Table S2. Displacements (in Ångstrom) among relevant stationary structures located by CAM-B3LYP/SVP calculations on the dimer and on the monomer, or predicted by the vibronic model. For the monomer minC_2 is the geometry it assumes in the C_2 stationary point on the S_1 and S_2 PES of the dimer according to the vibronic model (see expressions at the end of Section 1.1 of this SI)

<table>
<tr><td>dimer minS_1-C_2 − minS_0</td><td>monomer minC_2 − minS_0</td></tr>
<tr><td> 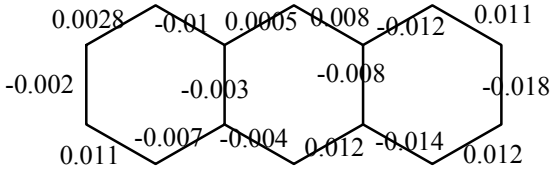
</td><td> 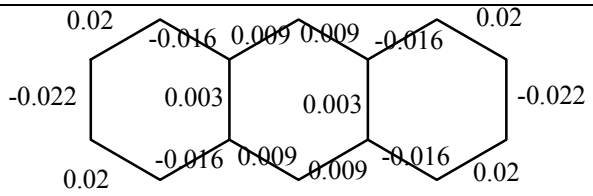
</td></tr>
<tr><td>dimer minS_1-loc − minS_0</td><td>monomer minS_1 − minS_0</td></tr>
<tr><td> 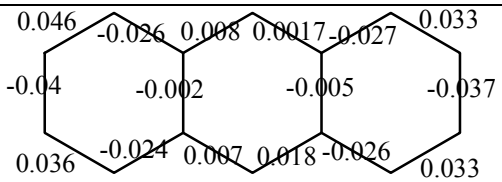
</td><td> 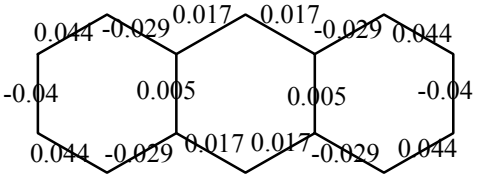
</td></tr>
<tr><td colspan="2">dimer minS_2-C_2 – minS_1-C_2</td></tr>
<tr><td colspan="2"> 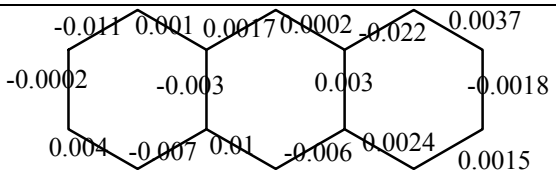
</td></tr>
</table>

Table S3. Comparison of the monomer electric transition dipoles computed at the ground-state geometry (FC), with the dimer transition dipole obtained from the model at the ground-state geometry (minS_0-*model*) and L_2 (minL_2) minima, or directly at TD-DFT level at minS_0 and minS_1-*loc*. CAMB3LYP/SVP calculations

Dipole	x	Y	z	module
		monomer values		
$\boldsymbol{\mu}_1$	-0.874	-0.271	-0.349	0.993
$\boldsymbol{\mu}_2$	0.874	0.271	-0.349	0.993
		dimer values from vibronic model		
		minS_0-*model*		
$\boldsymbol{\mu}_{D+}$	0	0	-0.544	0.544
$\boldsymbol{\mu}_{D-}$	1.236	0.384	0	1.294
		minL_2		
$\boldsymbol{\mu}_{D+}$	0.805	0.250	-0.413	1.060
$\boldsymbol{\mu}_{D-}$	-0.938	-0.291	-0.354	0.921
		TD-DFT calculations on the dimer		
		minS_0		
$\boldsymbol{\mu}_{S1}$	0	0	-0.477	0.477
$\boldsymbol{\mu}_{S2}$	1.162	0.692	0	1.352
		minS_1-*loc*[*]		
$\boldsymbol{\mu}_{S1}$	0.787	$\boldsymbol{\mu}_{S1}$	0.787	$\boldsymbol{\mu}_{S1}$
$\boldsymbol{\mu}_{S2}$	-0.904	$\boldsymbol{\mu}_{S2}$	-0.904	$\boldsymbol{\mu}_{S2}$

[*]between the two degenerate minima we selected the one corresponding to an excitation mainly on the chromophore "2"

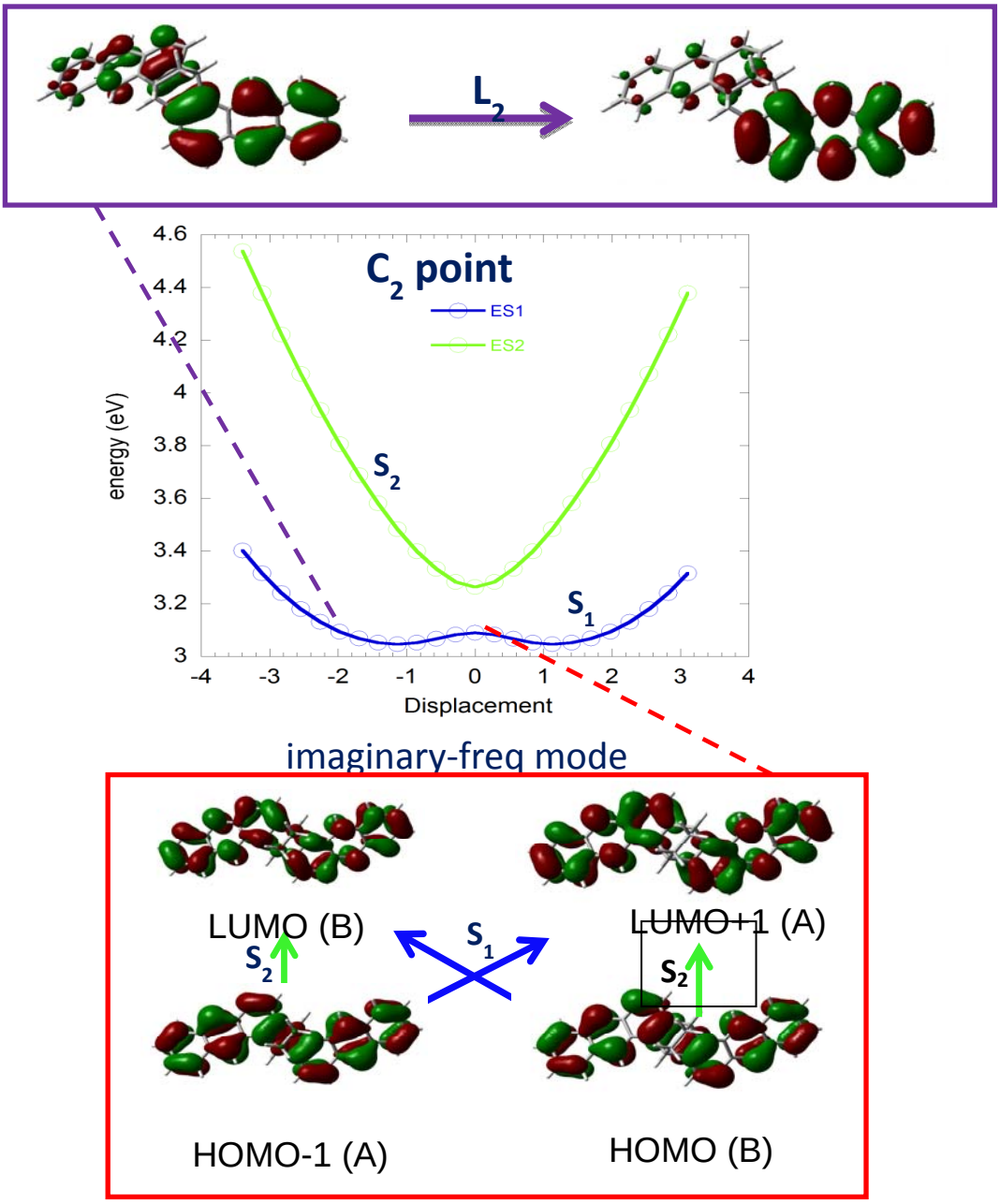

Figure S1. Central panel: S_1 and S_2 energy profiles along the S_1 imaginary frequency normal mode at the minS_1-C_2 structure, computed at CAM-B3LYP/SVP level of theory. All the other degrees of freedom were frozen at the minS_1-C_2 structure; displacements are given in dimensionless coordinates (ω=1820 cm^{-1}). **Top panel**: sketch of the Molecular Orbitals (MOs) involved in the transition in S_1 distorted minimum (the minimum corresponding to L_2, the local excitation on the right ("2") chromophore, has been selected). **Bottom panel:** sketch of the MOs involved in the transition in C_2 stationary point (the irreducible representation they belong to is indicated).

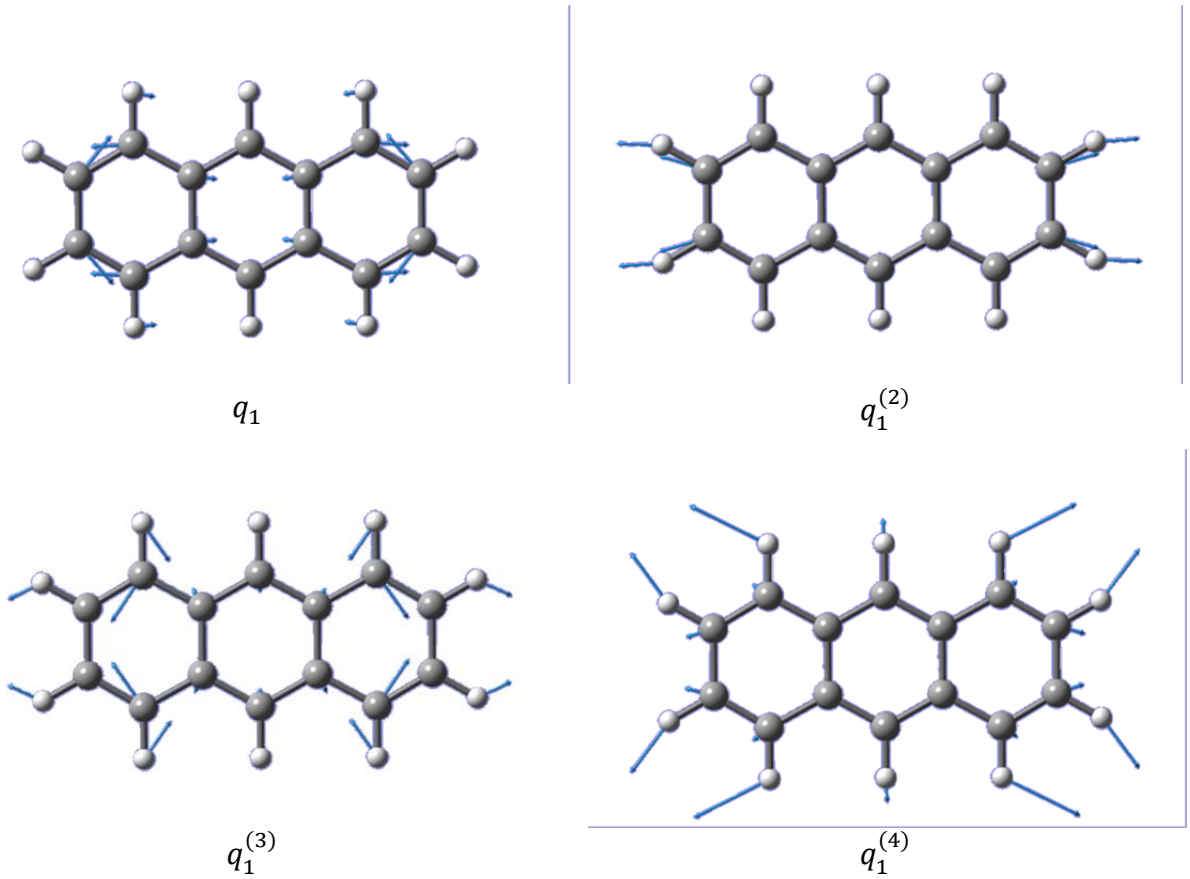

Figure S2. Effective modes for one of the two monomers computed from the LVC Hamiltonian with parameters obtained at CAM-B3LYP/SVP level of theory. In the labels blocks are specified by superscripts (omitted for the first-block) while the order within each block is indicated by a subscript. The first block of the LVC hierarchy (dimension 2) is made up by the mode depicted in top-left panel together with its symmetric counterpart on the other monomer. Analogously, second, third and fourth blocks of hierarchy (each of them with dimension 2) are made up by the modes depicted in the top-right, bottom-left and bottom-right panels, for each of the two monomers, respectively.

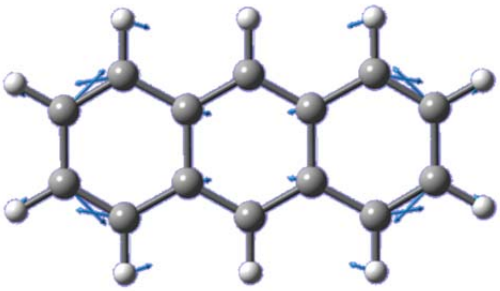

q_1

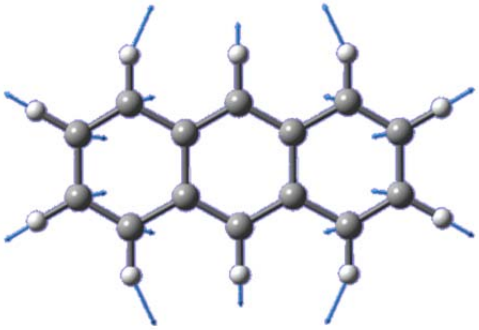

$q_1^{(2)}$

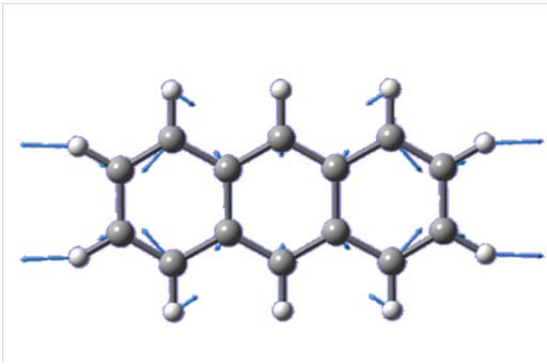

$q_2^{(2)}$

Figure S3. Effective modes for one of the two monomers computed from the QVC Hamiltonian with parameters obtained at CAM-B3LYP/SVP level of theory. In the labels blocks are specified by superscripts (omitted for the first-block) while the order within each block is indicated by a subscript. The first block of the QVC hierarchy (dimension 2) is made up by the mode depicted in top panel together with its symmetric counterpart on the other monomer. The second block of the hierarchy (dimension 4) is made up by the modes depicted in central and bottom panels for each of the two monomers.

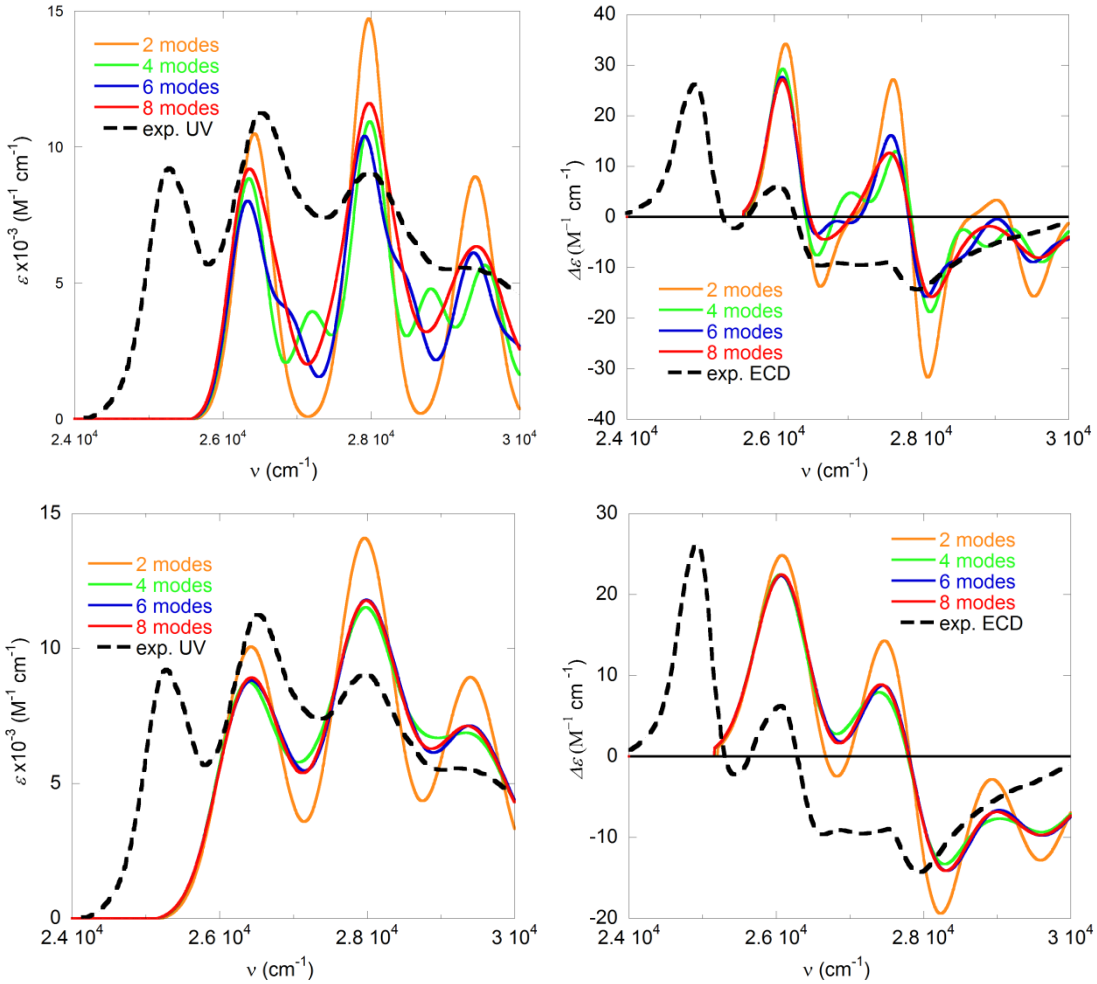

Figure S4. Absorption (left) and ECD (right) spectra computed according to LVC model on the ground of PBE0/SVP monomer parameters. Reported spectra have been computed with 8 coordinates, convoluted with a Gaussian with HWHM=250 cm^{-1} (CAM-B3LYP energetic parameters) and scaled to fit the experimental spectrum, which is also given for comparison.

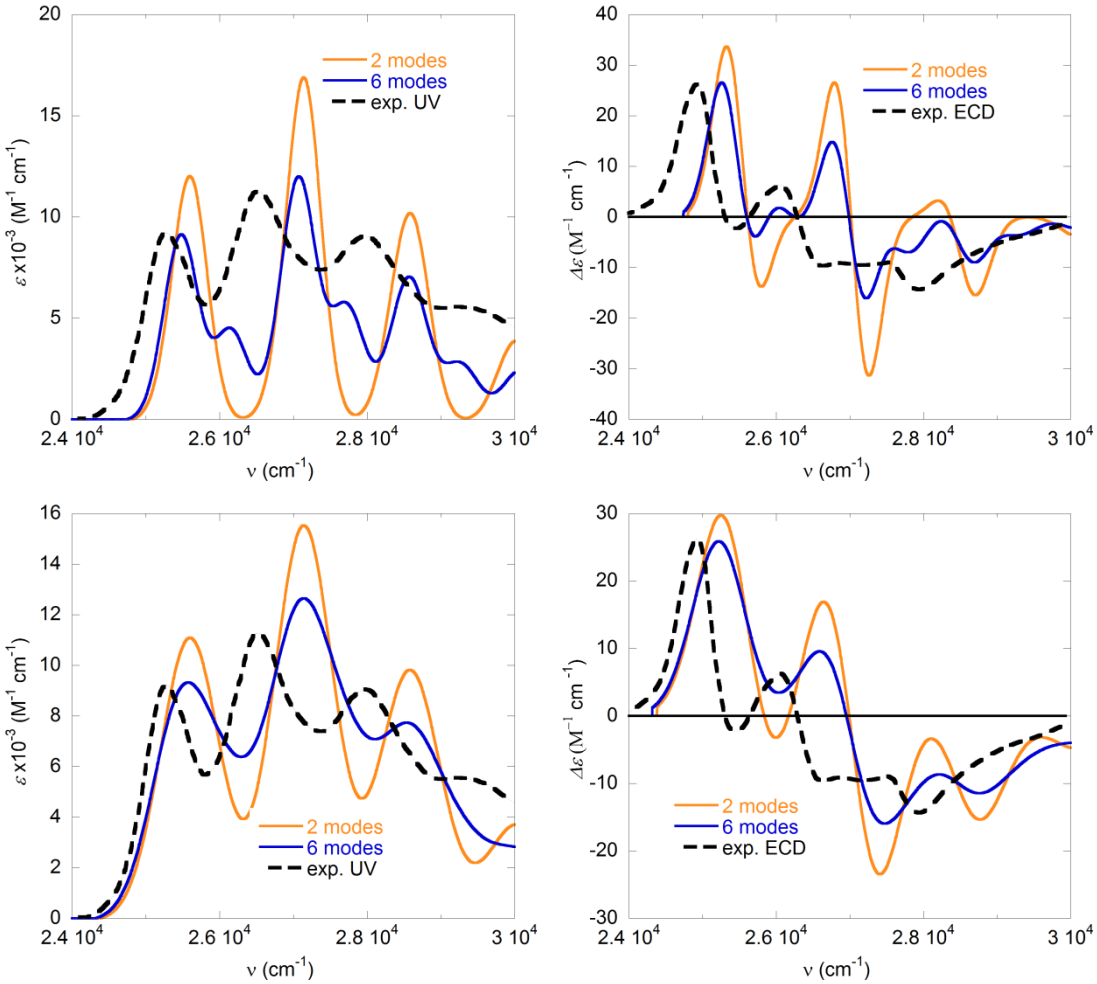

Figure S5. Absorption (left) and ECD (right) spectra computed according to QVC model on the ground of PBE0/SVP monomer parameters**.** Reported spectra have been computed for different truncations of the transformed Hamiltonian (first block 2 coordinates, first-second block 6 coordinates), convoluted with a Gaussian with HWHM=250 cm^{-1} (top) or HWHM=450 cm^{-1} (bottom) and blue-shifted by 2500 cm^{-1}. Intensities were computed in arbitrary units and the spectra were scaled to fit the experimental spectrum, which is also given for comparison. Comparing Figure S4 and S5 it can be noticed that as for the case of CAM-V3lYP/svp simulations, accounting for Duschinsky effects (QVC PBE0 Hamiltonian) do not significantly alter the main features of the LVC spectra.

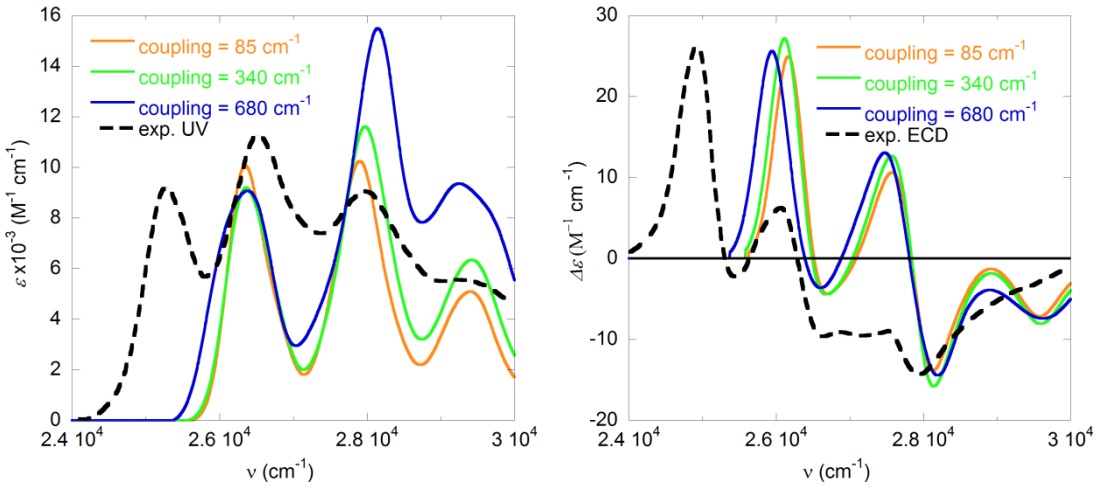

Figure S6. Absorption (left) and ECD (right) spectra computed according to LVC model on the ground of PBE0/SVP monomer parameters for different values of the exciton coupling (V_{12}=85, 340 and 680 cm^{-1}). Reported spectra have been computed in arbitrary units with 8 coordinates, convoluted with a Gaussian with HWHM=250 cm^{-1} and scaled to fit the experimental spectrum, which is also given for comparison. Notice that the scaling factor given in the inset is different for each choice of V_{12}, since it alters the total intensity carried by the spectra. It can be noticed that increasing the coupling to -680 cm^{-1} produces a remarkable increase of the splitting of the vibronic bands (750 and 850 cm^{-1} in ECD and 1940 cm^{-1} in absorption) worsening the agreement with experiment; on the contrary the reduction of the coupling to -85 cm^{-1} reduces the splitting slightly (715 and 735 cm^{-1} in ECD and 1530 cm^{-1} in absorption), only modestly improving the comparison with experiment.

Complete Gaussian 09 Reference:

Frisch, M. J.; Trucks, G. W.; Schlegel, H. B.; Scuseria, G. E.; Robb, M. A.; Cheeseman, J. R.; Scalmani, G.; Barone, V.; Mennucci, B.; Petersson, G. A.; Nakatsuji, H.; Caricato, M.; Li, X.; Hratchian, H. P.; Izmaylov, A. F.; Bloino, J.; Zheng, G.; Sonnenberg, J. L.; Hada, M.; Ehara, M.; Toyota, K.; Fukuda, R.; Hasegawa, J.; Ishida, M.; Nakajima, T.; Honda, Y.; Kitao, O.; Nakai, H.; Vreven, T.; Montgomery, Jr., J. A.; Peralta, J. E.; Ogliaro, F.; Bearpark, M.; Heyd, J. J.; Brothers, E.; Kudin, K. N.; Staroverov, V. N.; Kobayashi, R.; Normand, J.; Raghavachari, K.; Rendell, A.; Burant, J. C.; Iyengar, S. S.; Tomasi, J.; Cossi, M.; Rega, N.; Millam, J. M.; Klene, M.; Knox, J. E.; Cross, J. B.; Bakken, V.; Adamo, C.; Jaramillo, J.; Gomperts, R.; Stratmann, R. E.; Yazyev, O.; Austin, A. J.; Cammi, R.; Pomelli, C.; Ochterski, J. W.; Martin, R. L.; Morokuma, K.; Zakrzewski, V. G.; Voth, G. A.; Salvador, P.; Dannenberg, J. J.; Dapprich, S.; Daniels, A. D.; Farkas, Ö.; Foresman, J. B.; Ortiz, J. V.; Cioslowski, J.; Fox, D. J. *Gaussian 09, Revision A.1* **2009**.